Supplementary Information

Morphology-Controlled Fe_3O_4@CNF Nanocomposites for Sustainable Paper-Based Energy Storage with Recyclability

Iqra Rabani[a,b*], Tanveer Hussain[c], Ajeet Kumar[d], Ghulam Dastgeer[e], Faheem Maqsood[a], Karolien De Wael[b], and Young-Soo Seo[a*]

[a]Department of Nanotechnology and Advanced Materials Engineering, Sejong University, Seoul 05006, Republic of Korea

[b]Antwerp engineering, photoelectrochemistry and sensing (A-PECS), University of Antwerp, Groenenborgerlaan 171, 2020 Antwerp, Belgium

[c]School of Science and Technology, University of New England, Armidale, New South Wales, 2351, Australia

[d]Department of Mechanical Engineering, 3.04, 4 East,University of Bath, Claverton Down

Bath, BA2 7AY, United Kingdom

[e]Department of Physics and Astronomy, Sejong University, Seoul 05006, Republic of Korea

*Equal Corresponding author E-mail: iqrarabani@sejong.ac.kr & ysseo@sejong.ac.kr

Figure Contents:

Figure S3. *TEM micrograph for the CNF.*

Figure S4. *XRD pattern for the CNF.*

Figure S5(a-d). *Cyclic Voltammetry (CV) profiles at the diverse scan rates ranging from 10-100 mV/s for the* ***(a)*** *Fe_3O_4@CNF1,* ***(b)*** *Fe_3O_4@CNF2 and* ***(c)*** *Fe_3O_4@CNF3. Galvanostatic charging-discharging (GCD) profiles at the various current densities ranging from 0.5 to 10 A/g for the* ***(d)*** *Fe_3O_4@CNF1,* ***(e)*** *Fe_3O_4@CNF2* ***(f)*** *Fe_3O_4@CNF3 nanocomposites.*

Figure S6. ***(a-b)*** *CV profiles for the Fe_3O_4 NPs and CNF at diverse scan rates, respectively and* ***(c-d)*** *GCD profiles for Fe_3O_4 NPs and CNF at different current densities, respectively.*

Figure S7(a-b). *CV profiles for the CNF and Fe_3O_4 NPs at diverse scan rates, respectively (Symmetric supercapacitor performance; two electrode measurement).*

Figure S8(a-b). *GCD profiles for the CNF and Fe_3O_4 NPs at the diverse current density, respectively (Symmetric supercapacitor performance; two electrode measurement).*

Figure S9. ***(a)*** *Tensile strength and elongation at break and* ***(b)*** *CV profiles at the 10 mV/s of scan rate for the series of the compositions comprises Fe_3O_4@CNF1 (2:1:: Fe_3O_4:CNF at 25 ˚C), Fe_3O_4@CNF2 (1.5:1:: Fe_3O_4:CNF at 25 ˚C), Fe_3O_4@CNF3 (1:1:: Fe_3O_4:CNF at 60 ˚C) and Fe_3O_4@CNF4 (1:1:: Fe_3O_4:CNF at 100 ˚C) nanocomposite papers.*

Figure S10. ***(a-b)*** *Photo digital images for the Fe_3O_4@CNF4 nanocomposite before and after carbonization and the assembly of the symmetric supercapacitor device and* ***(c-d)*** *The tensile strength at break and CV profiles at the 10 mV/s of scan rate for the Fe_3O_4@CNF4 before and after carbonization.*

Figure S11. ***(a)*** *GCD profiles at 5 A/g of current density under varying voltage windows and* ***(b)*** *Coulombic efficiency vs. voltage, stable at 97.1% up to 1.2 V and dropping to 92% at 1.4 V due to electrolyte decomposition.*

References

S-1. Materials and Instrumentations

Cellulose nanofiber (CNF) was purchased by Moorim P&P resided in Ulsan, Korea. The ferric chloride hexahydrate ($FeCl_3.6H_2O$, 98%, MW = 270.3), ferrous chloride tetrahydrate ($FeCl_2.4H_2O$, 99%, MW = 198.81), anhydrous ethanol (CH_3CH_2OH, 99.5%, MW = 46.07), ammonia (NH_3, 28%, MW = 17.031), Furfuryl alcohol (FFA, 99%, MW = 98.1), p-benzoquinone (BQ, 99%, MW = 108.09) and Ammonium oxalate (AO, 99%, MW = 124.1) were purchased from the sigma Aldrich, Korea. Carbon black (95%, MW = 12.01), polyvinylidene fluoride (PVDF, 98%, MW = 180,000), N-Methyl-2-pyrrolidone (NMP; 99%, MW = 99.13) were purchased from the sigma Aldrich, South Korea.

The crystal lattice was studied using X-ray diffraction (XRD; Panalytical). The spectra were recorded using Cu Kα radiation (λ = 0.15418 nm) at 30 mA and 40 kV in the 2θ range of 10° to 80° with a scanning speed of 2°/min. The morphological analysis was further shown by using the field-emission scanning electron microscope (FESEM; TESCAN Mira3) and Transmission electron microscopy (TEM; JEM 2010 FEF (UHR)). In addition, the detailed microstructure, as well as elemental mapping, were evaluated by using high-resolution transmission electron microscopy (HRTEM) and energy-dispersive X-ray spectroscopy by using the same stated TEM instruments by altering the mode. For the sample preparation procedure for the TEM measurement; the synthesized samples were dissolved into the absolute ethanol solution and then ultrasonicated for 5 min. Approximately, 0.5 μL drop was added to the carbon grid

and then dried in the vacuum oven overnight at 100 ˚C. The electronic chemistry and valance states were characterized by employing the X-ray photoelectron spectroscopy (XPS; ESCALAB 250Xi (Thermo Scientific). X-ray photoelectron spectrometer with monochromatic Al Kα (1486.6 eV) radiation as the excitation source). The surface area measurements of the synthesized samples were described through Brunauer−Emmett−Teller (BET) and Barrett−Joyner−Halenda (BJH) methods using the Quantachrome NOVA 2000e sorption analyzer at liquid nitrogen temperature (77 K). An electrochemical potentiostat (BioLogic SP 150) was employed to perform the electrochemical test on the CNF, Fe_3O_4, and Fe_3O_4@CNF devices.

S-2 Calculations of the specific capacity, Trasattis's and Dunn's method

The specific capacity (C_s) in F/g was calculated from galvanostatic discharge curves as:

$$C_s = \frac{2 \times I}{m\Delta V}\int V dt \quad \text{---------- (1)}$$

where m is the mass of active material (mg), and I is the current in mA, ΔV is the voltage window and $\int V dt$ is the area under the discharge curve[1]. Then, we utilized Trasattis's method [2] (equation S1) to dissect the total stored charge into capacitive and diffusion-controlled contributions from the plots of 1/Qs vs. √(scan rate) and Qs vs. 1/√(scan rate) (Potential window is 0.5 and 1.0 V and Qs = specific capacitance, C_{sp})

$$Q_t = Q_{cap} + Q_{diff} \quad \text{---------- (2)}$$

Where, Qt is total charge storage capacity (capacitance), Qcap is capacitive mechanisms (surface-controlled capacitance) and Qdiff is diffusion-controlled processes (diffusion-controlled capcitance).

To determine the charge storage contribution, we applied the following modified power law or Dunn's method [3] equation S2.

$$\frac{iV}{v^{0.5}} = K_1 v^{0.5} + K_2 \quad \text{---------- (3)}$$

Where, (*iV*) is the response current having values at current peak (i) and applied voltage window (V) and v is the scan rate. K_1 and K_2 are the slope and intercepts of the line after plotting graph between $\frac{iV}{v^{0.5}}$ and $v^{0.5}$ [4, 5]. For the full device, we use peak potentials at 0.5 V (oxidation and reduction peak potentials).

S-3 Calculations of the symmetric supercapacitor capacitance, capacity retention, columbic efficiency, energy and power density

$$C_s = \frac{(2 \times I \times \Delta t)}{m \times \Delta V} \quad \text{----------(4)}$$

Wherein:

- I is the discharge current (A),
- Δt is the discharge time (s),
- m is the mass of active material (g),
- ΔV is the potential window (V).

The **retention (%)** is then calculated as:

$$\text{Retention (\%)} = \frac{C_{final}}{C_{initial}} \times 100 \text{----------(5)}$$

Where, C_{final} = Specific capacitance at the 1st cycle

$C_{initial}$ = Specific capacitance at the last cycle.

$$\text{Columbic efficiency (\%)} = \frac{t_{discharge}}{t_{charge}} \times 100 \text{----------(6)}$$

Wherein,

$t_{discharge}$: discharge time (in s)

t_{charge}_: charge time (in s)

$$\text{Energy density} = \left(\frac{C \times (\Delta V)^2}{8}\right) \text{----------(7)}$$

$$\text{Power density} = \left(3600 \times \frac{E}{\Delta t}\right) \text{----------(8)}$$

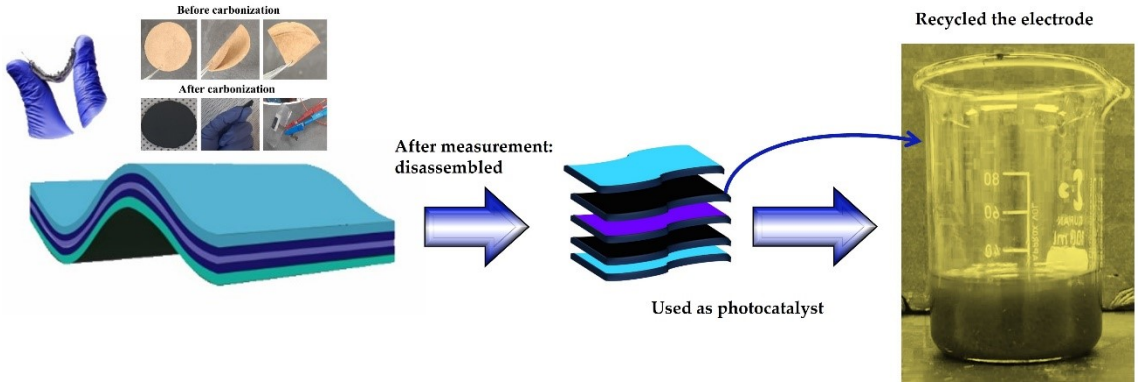

Figure S1. *Schematic representation and experimental procedure for reusing the Fe_3O_4@CNF_4-based paper electrode.*

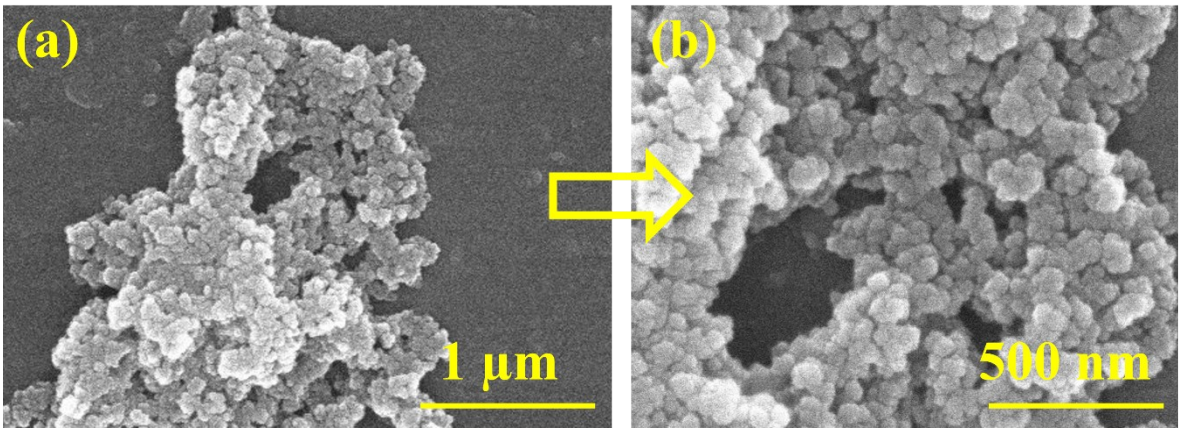

Figure S2. (a-b) *FESEM micrographs of the Fe_3O_4 NPs at high and low magnifications.*

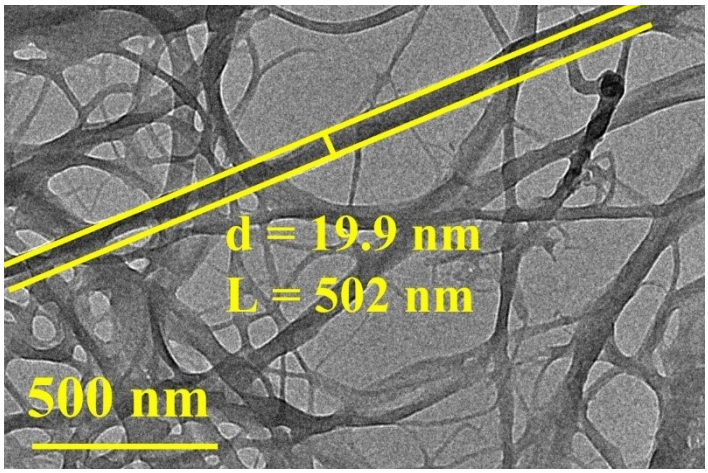

Figure S3. *TEM micrograph for the CNF.*

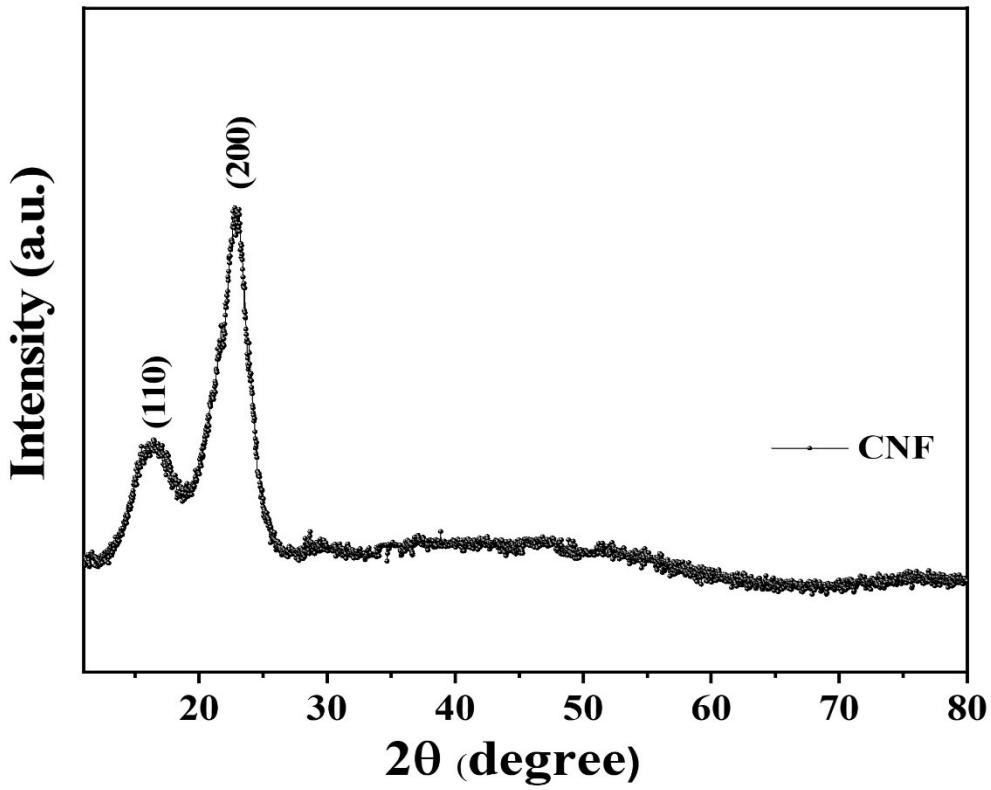

Figure S4. *XRD pattern for the CNF.*

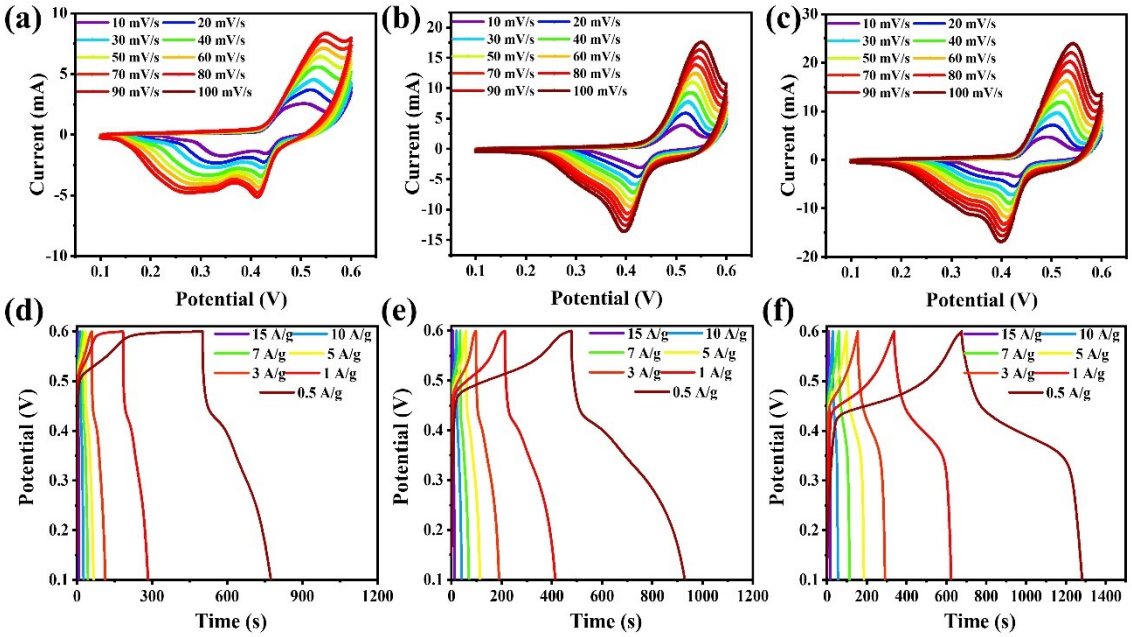

Figure S5(a-d). *Cyclic Voltammetry (CV) profiles at the diverse scan rates ranging from 10-100 mV/s for the* ***(a)*** *Fe_3O_4@CNF1,* ***(b)*** *Fe_3O_4@CNF2 and* ***(c)*** *Fe_3O_4@CNF3. Galvanostatic charging-discharging (GCD) profiles at the various current densities ranging from 0.5 to 10 A/g for the* ***(d)*** *Fe_3O_4@CNF1,* ***(e)*** *Fe_3O_4@CNF2* ***(f)*** *Fe_3O_4@CNF3 nanocomposites.*

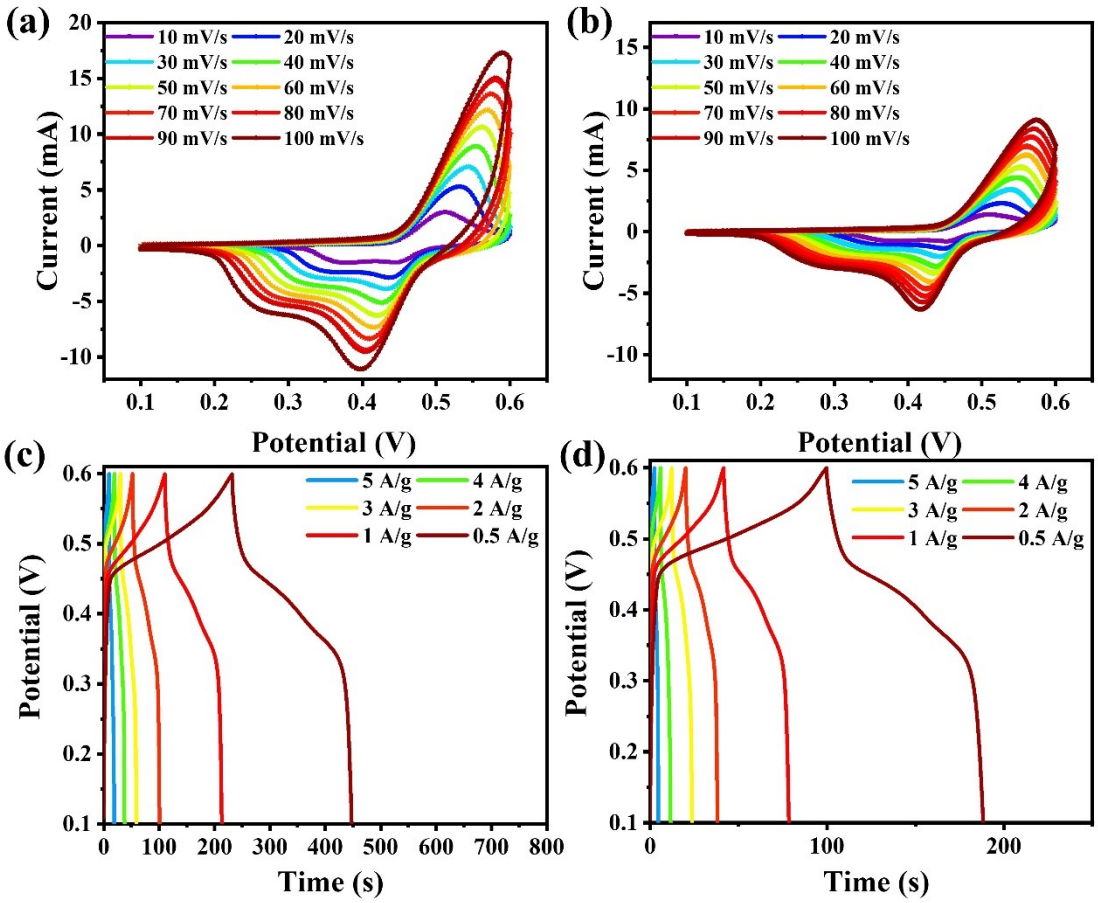

Figure S6. (a-b) *CV profiles for the Fe_3O_4 NPs and CNF at diverse scan rates, respectively and* ***(c-d)*** *GCD profiles for Fe_3O_4 NPs and CNF at different current densities, respectively.*

Table S1. *Comparison of charge transfer resistance (Rct) values for various electrode compositions under three-electrode and symmetric supercapacitor configurations, indicating improved conductivity with Fe_3O_4@CNF4 composite.*

Electrode Composition	R_{ct} (Ω) – Three-Electrode Setup	R_{ct} (Ω) – Symmetric Supercapacitor
CNF (pristine)	22.1	26.4
Fe_3O_4 NPs	8.2	13.4
Fe_3O_4@CNF1	18.2	
Fe_3O_4@CNF2	14.0	
Fe_3O_4@CNF3	11.2	
Fe_3O_4@CNF4	4.5	7.5

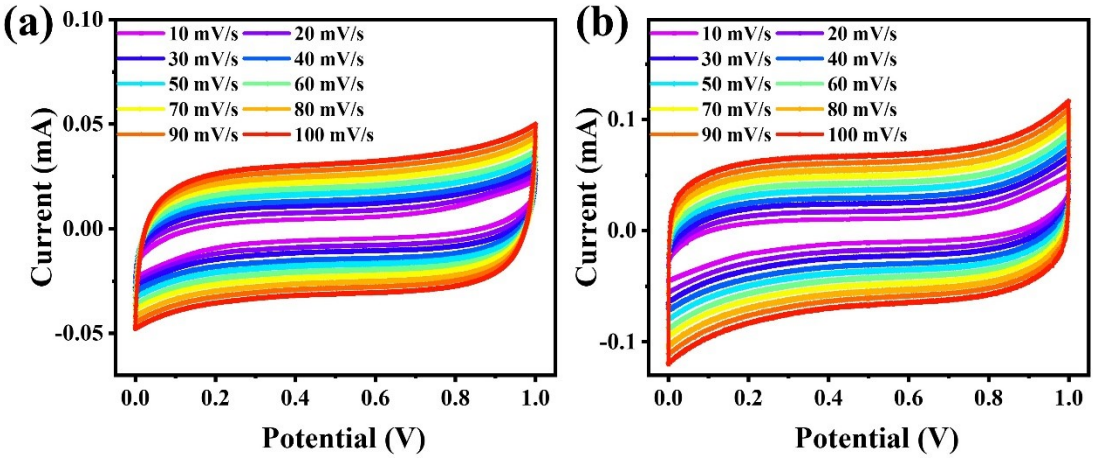

Figure S7(a-b). *CV profiles for the CNF and Fe_3O_4 NPs at diverse scan rates, respectively (Symmetric supercapacitor performance; two electrode measurement).*

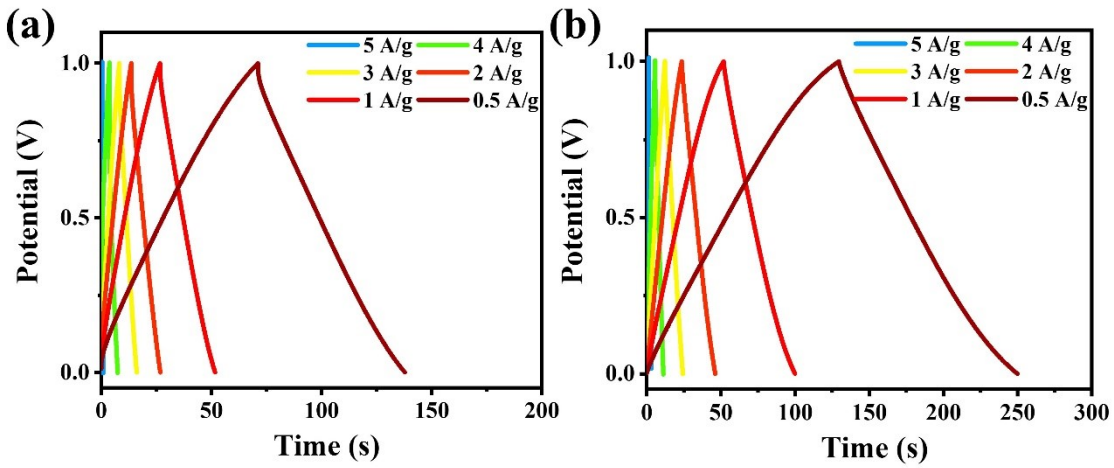

Figure S8(a-b). *GCD profiles for the CNF and Fe_3O_4 NPs at the diverse current density, respectively (Symmetric supercapacitor performance; two electrode measurement).*

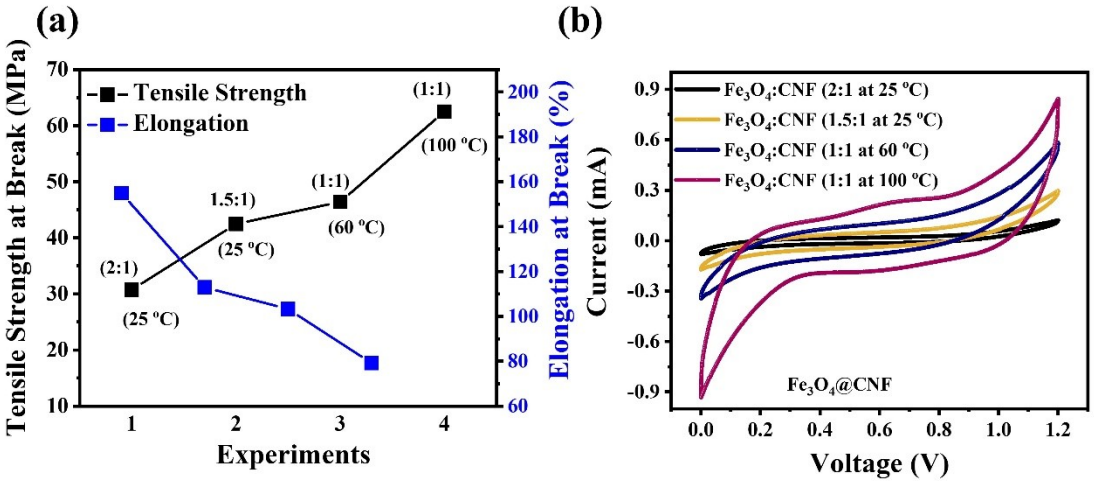

Figure S9. (a) *Tensile strength and elongation at break and* ***(b)*** *CV profiles at the 10 mV/s of scan rate for the series of the compositions comprises Fe_3O_4@CNF1 (2:1:: Fe_3O_4:CNF at 25 ˚C), Fe_3O_4@CNF2 (1.5:1:: Fe_3O_4:CNF at 25 ˚C), Fe_3O_4@CNF3 (1:1:: Fe_3O_4:CNF at 60 ˚C) and Fe_3O_4@CNF4 (1:1:: Fe_3O_4:CNF at 100 ˚C) nanocomposite papers.*

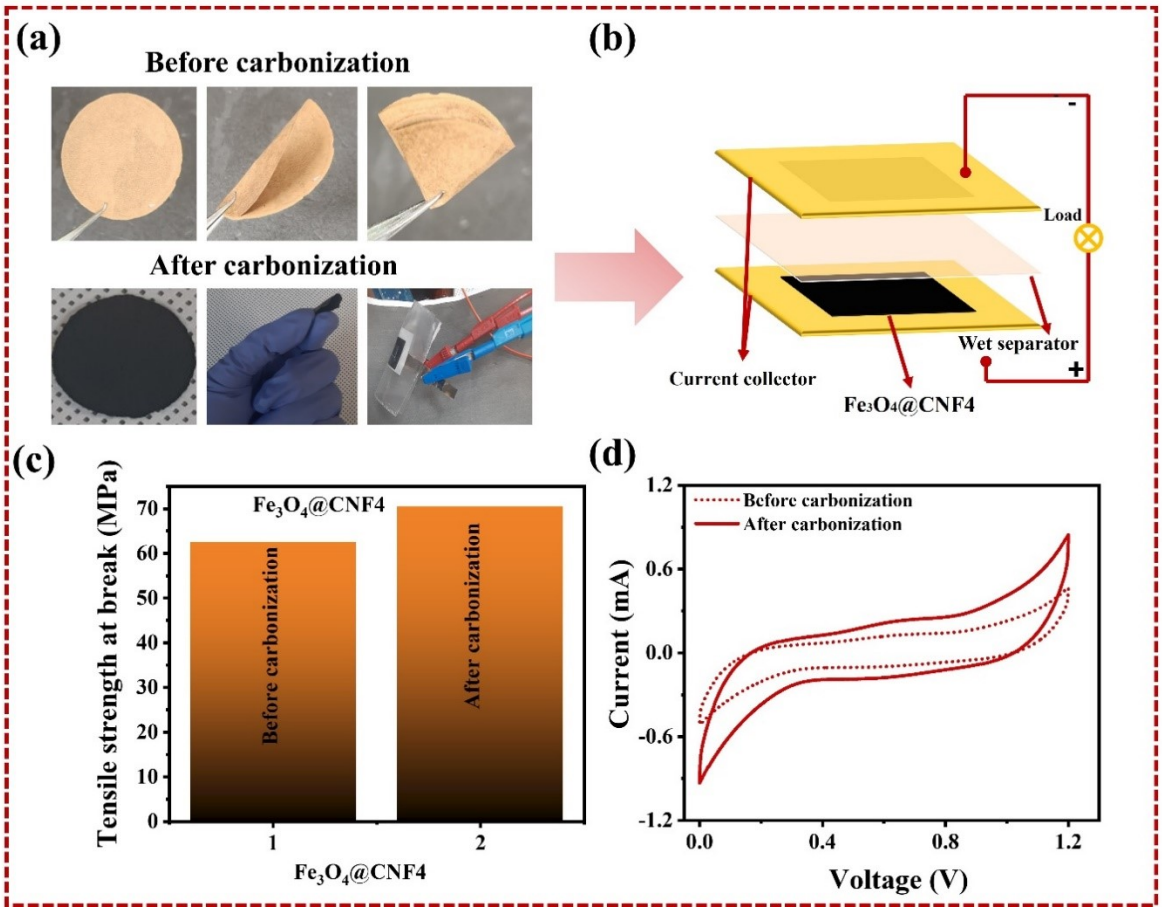

Figure S10. (a-b) *Photo digital images for the Fe_3O_4@CNF4 nanocomposite before and after carbonization and the assembly of the symmetric supercapacitor device and* ***(c-d)*** *The tensile strength at break and CV profiles at the 10 mV/s of scan rate for the Fe_3O_4@CNF4 before and after carbonization.*

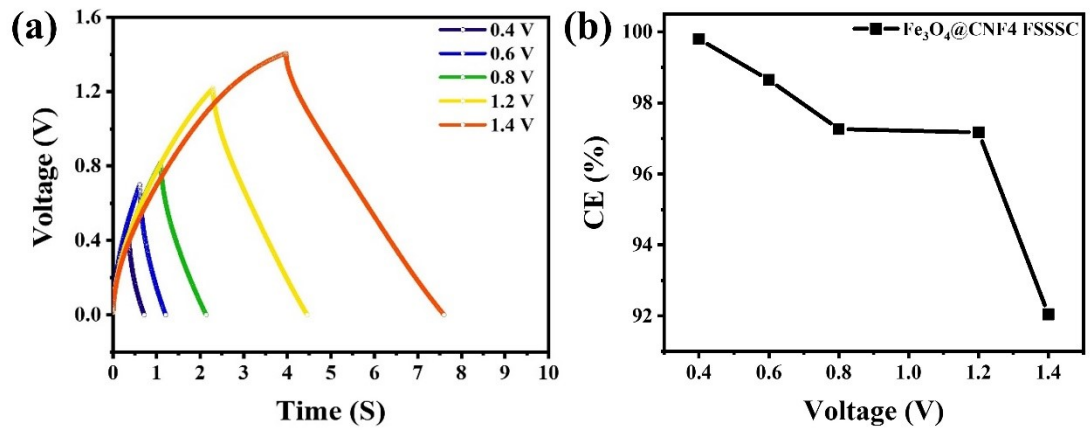

Figure S11. (a) *GCD profiles at 5 A/g of current density under varying voltage windows and* ***(b)*** *Coulombic efficiency vs. voltage, stable at 97.1% up to 1.2 V and dropping to 92% at 1.4 V due to electrolyte decomposition.*

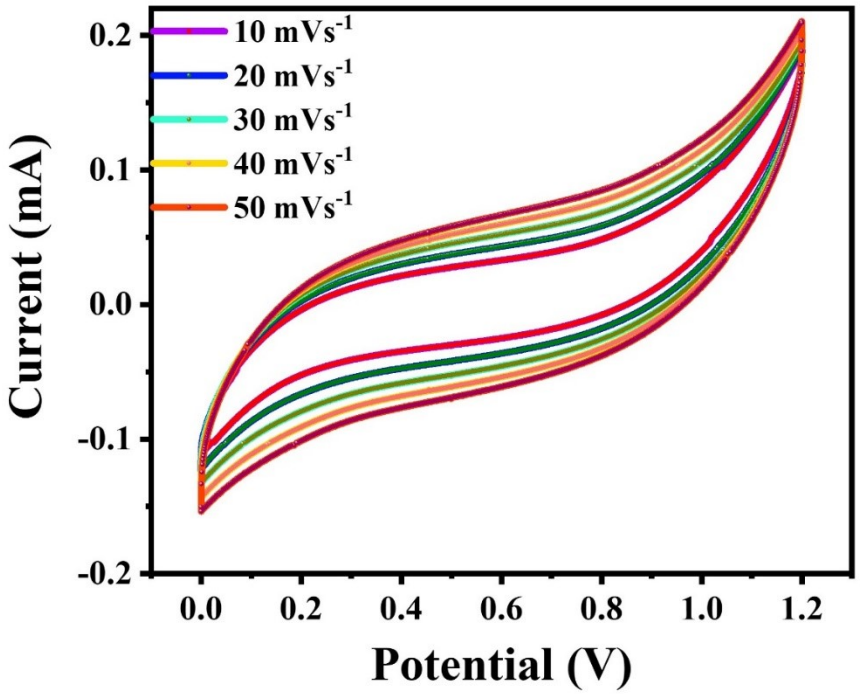

Figure S12. *CV profiles for the CNF FSSSCs at diverse scan rate, respectively (Symmetric supercapacitor performance; two electrode measurement).*

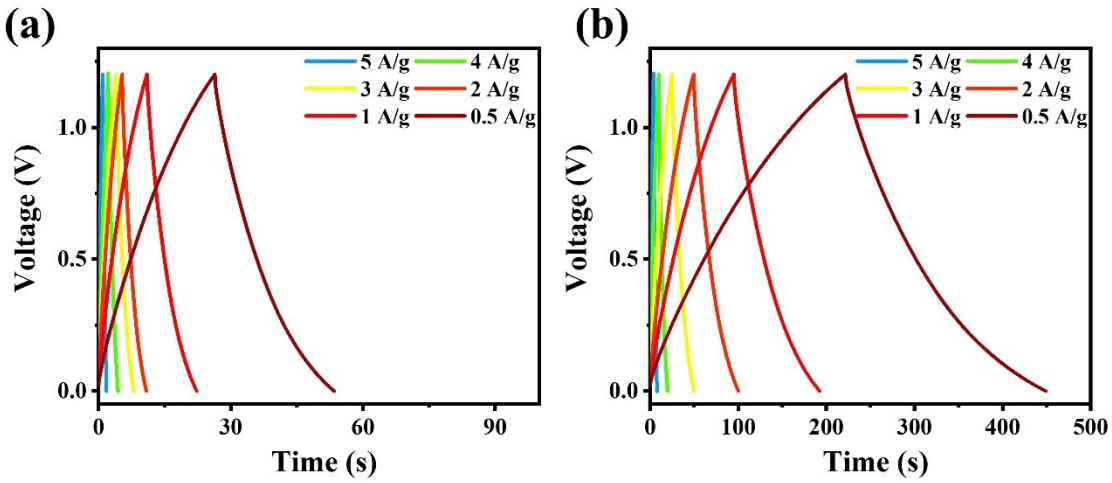

Figure S13. *GCD profiles for the* ***(a)*** *CNF and* ***(b)*** *Fe_3O_4@CNF FSSSCs at diverse current density, respectively (Symmetric supercapacitor performance; two electrode measurement*).

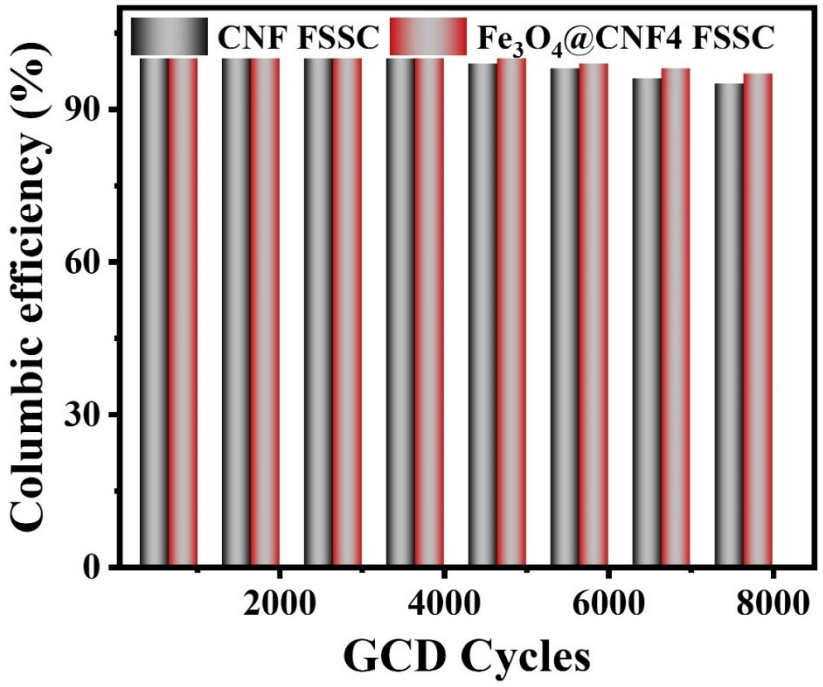

Figure S14. *Coulombic efficiency (%) again GCD cycles for the Fe_3O_4@CNF FSSSC and CNF FSSSC at 5 A/g of current density.*

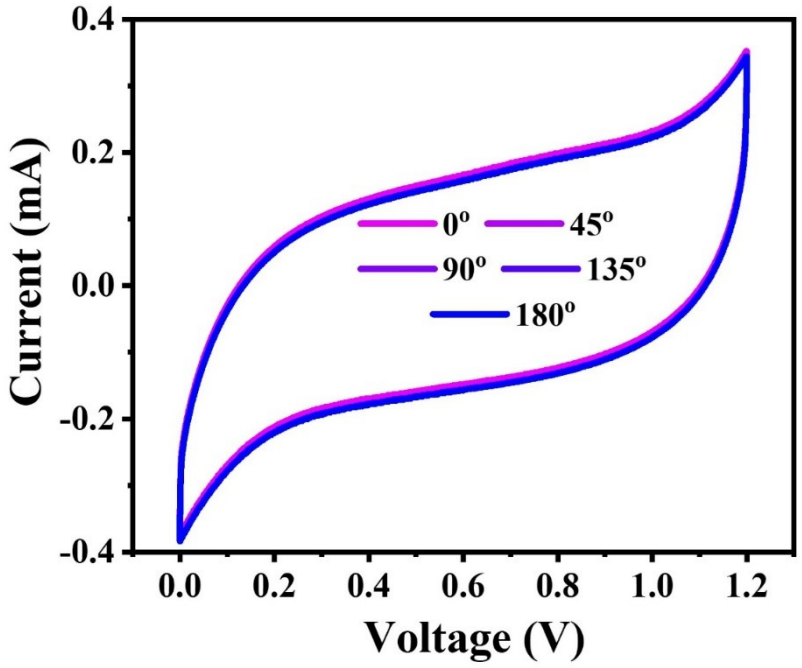

Figure S15. *CV profiles for the Fe_3O_4@CNF FSSSCs at various bending states for optimizing the flexibility.*

Table S2. Comparative electrochemical performance of Fe_3O_4@CNF nanocomposite in the three-electrode system with other previously reported materials.

Electrode materials	Electrolyte	Voltage window (V)	Specific capacitance	Ref.
Fe_3O_4@CNF4	**3 M KOH**	**0.1 to 0.6**	**2046.32 $F.g^{-1}$ at 0.5 $A.g^{-1}$**	**Present work**
Fe_3O_4 NPs	**3 M KOH**	**0.1 to 0.6**	**410.34 $F.g^{-1}$ at 0.5 $A.g^{-1}$**	
CNF	**3 M KOH**	**0.1 to 0.6**	**172.98 $F.g^{-1}$ at 0.5 $A.g^{-1}$**	
Co_3O_4@CNF	3 M KOH	-0.2 to 0.6	789.9 $F.g^{-1}$ at 1 $A{\cdot}g^{-1}$	6
$ZnMn_2O_4$/C	6 M KOH	0 to 1.2	589 $F.g^{-1}$ at 1 $A{\cdot}g^{-1}$	7
ZnO/MnO	1 M Na_2SO_4	0 to 0.8	14 mF/cm^2 at 0.1 mA/cm^2	8
ZnO/MnO_2 nanowires	1 M Na_2SO_4	0 to 0.9	501 $F.g^{-1}$ at 2 $A{\cdot}g^{-1}$	9
$ZnMn_2O_4$/carbon	6 M KOH	-1 to -0.3	105 $F.g^{-1}$ at 0.3 $A{\cdot}g^{-1}$	10
ZnO nanocones	1 M KOH	0.1 to 0.6	236 $F.g^{-1}$ at 1 $A{\cdot}g^{-1}$	11

NCA/Co_3O_4	6 M KOH	-0.05 to 0.45	616 F·g^{-1} at 1.2 A·g^{-1}	[12]
$CuCo_2S_4$/CNT/graphene	1 M Na_2SO_4	0 to 0.6	504 F·g^{-1} at 10 A·g^{-1}	[13]
CPSC-3rGO	0.2 M Na_2SO_4	-0.2 to 0.8	446 F·g^{-1} at 1 A·g^{-1}	[14]
CS@ZnO Core-shell	6 M KOH	0 to 0.4	630 F·g^{-1} at 2 A·g^{-1}	[15]
Co_3O_4 nanoflakes@SrGO	2 M KOH	-0.2 to 0.5	406 F·g^{-1} at 1 A·g^{-1}	[16]
$CoMoO_4$ nanoclusters	6.0 M KNO_3	−0.9 to 0.6	367 F·g^{-1} at 1.2 A·g^{-1}	[17]
Ni-Co selenide	6 M KOH	0 to 0.6	742.4 F·g^{-1} at 1 mA cm^{-2}	[18]
$NiCo_2O_4$	6 M KOH	-0.2 to 0.6	225 C. g^{-1} at 0.5 A g^{-1}	[19]

Table S3. *Comparative electrochemical performance of symmetric supercapacitor devices with other previously reported materials.*

Device name	Type	Electrolyte	Specific capacitance	Stability /GCD cycling	Ref.
Fe_3O_4@CNF4	**Symmetric**	**3 M KOH**	**390 F/g @ 0.5 A/g**	**88%/8000**	**Present Work**
Fe_3O_4 NPs	**Symmetric**	**3 M KOH**	**122 F/g @ 0.5 A/g**	**75%/8000**	
CNF	**Symmetric**	**3 M KOH**	**67 F/g @ 0.5 A/g**	**80%/8000**	
CoNW/CF//CoNW/CF SSC	Symmetric	3.0 M KOH	517.33 mF/cm^3 @ 0.26 mA/ cm^2	95/5000	[20]
NCOs	Symmetric	1.0 M KOH	89 F g^{-1} @ 0.23 A.g^{-1}	-	[21]
ZnO/Co_3O_4-450//AC	Asymmetric	1.0 M KOH	153 F g^{-1} @ 1 A.g^{-1}	-	[22]
CC@NiC_2O_4 //CC@NC	Asymmetric	6.0 M KOH	89.7 F g^{-1} @ 1 A g^{-1}	86.7/20000	[23]
Co_3O_4@Ni_3S_2	Asymmetric	3.0 M KOH	126 F g^{-1} @ 1 A.g^{-1}	83.5/5000	[24]
Ag/NiO	Asymmetric	3.0 M KOH	204 C.g^{-1} @ 2.5 A.g^{-1}	96/4000	[25]
Co_3O_4@Ni(OH)2//AC	Asymmetric	6.0 M KOH	110 F.g^{-1} @ 2.5 A.g^{-1}	86/1000	[26]
MoS_2-NH_2/PANI nanosheets	Symmetric	1 M H_2SO_4	58.6 F g^{-1} @ 2 A.g^{-1}	96.5/10000	[27]
MoS_2/CNS	Symmetric	1 M Na_2SO_4	108 F g^{-1} @ 1 A.g^{-1}	-	[28]

MoS_2/G nanobelts	Symmetric	1 M Na_2SO_4	278.2 $F.g^{-1}$ @ 0.8 $A.g^{-1}$	-	[29]
MoS_2/rGO	Symmetric	1 M H_2SO_4	306 $F.g^{-1}$ @ 0.5 $A.g^{-1}$	-	[30]
NiS/MoS2@N-rGO	Symmetric	6 M KOH	1028 $F.g^{-1}$ @1 $A.g^{-1}$	94.5/50000	[31]
MoS_2/rGO	Symmetric	NaOH	323 $F.g^{-1}$ @ 0.2 $A.g^{-1}$	76.8/500	[32]

Table S4. *Comparative electrochemical performance of symmetric flexible supercapacitor devices with other previously reported materials.*

Device name	**Type**	**Electrolyte**	**Specific capacitance**	**Stability (%)/GCD cycling**	**Ref.**
Fe_3O_4@CNF4 FSSSCs	**Symmetric**	**PVA-KOH**	**188 $F.g^{-1}$@ 0.5$A.g^{-1}$**	**94/8000**	**Present work**
CNF FSSSCs	**Symmetric**	**PVA-KOH**	**23 $F.g^{-1}$@ 0.5$A.g^{-1}$**	**85/8000**	
BC/Porous GO	Symmetric	PVA/H_3PO_4	65.9 $F.g^{-1}$@ 0.4 $A.g^{-1}$	----	[33]
Cellulose/Graphite/PANI	Symmetric	PVA/H_3PO_4	357 F/g@ 80 mV/s	----	[34]
Cellulose/rGO/Ag/Fe_2O_3	Symmetric	PVA/LiCl	112 mF/cm^2@ 2 mA/cm^2	-----	[35]
Cellulose-Graphene	Symmetric	PVA-H_2SO_4	120 F/g	99/5000 cycles	[36]
3D graphene-MoS_2 hybrid	Symmetric	KOH/PVA	58.0$F.g^{-1}$@ 2 $A.g^{-1}$	-	[37]
TaS_2	Symmetric	PVA/LiCl	508 F/cm^3 @ 10 mV/s	92/4000	[38]
Cu_2WS_4	Symmetric	PVA/LiCl	583.3 F cm^{-3} @ 0.31 A cm^{-3}	95/3000	[39]
SS/MWCNTs/$MoTe_2$	Symmetric	PVA-$LiClO_4$	68.01 $F.g^{-1}$ @ 0.2 $mA.cm^{-2}$	94/2000	[40]
MWCNTs/$MoSe_2$	Symmetric	PVA-KOH	27 $F.g^{-1}$ @ 0.4 A/g	95/1000	[41]

MoS_2/carbon cloth	Symmetric	PVA-$LiClO_4$	368 $F.g^{-1}$ @ 5 mV/s	96.5/5000	[42]
MoS_2/NPG	Symmetric	1 M Na_2SO_4	102.5 F g^{-1} @ 1 A g^{-1}	91.67/5000	[43]
VSL-MoS2@3D-Ni foam	Symmetric	Na_2SO_4/PVA	34.1 $F.g^{-1}$@ 1.3 $A.g^{-1}$	82.5/10000	[44]

Table S5: *Comparative outcomes for the previously reported photocatalysts with our present results employing the various dye/pollutant.*

Photocatalyst	**Dye/Pollutant**	**Degradation efficiency (%) /Time (min)**	**Catalyst dose (mg/L)**	**Reference**
Recycles Fe_3O_4@CNF4 FSSSCs	**CV**	**95/45**	**100**	**Present work**
α -MnO_2-Fe_3O_4	Methylene Blue	**94.8/120**	**20**	[45]
Porous t-$CuFe_2O_4$	Acid fuchsin	80/90	---	[46]
δ-MnO_2/ montmorillonite	Methylene Blue	92/700	2000	[47]
δ-MnO_2	Methylene Blue	99/700	2000	[47]
MnO_2	Methylene Blue	93/180	200	[48]
MnO_2/Fe_3O_4	Methylene Blue	98.2/180	200	[48]
MnO_2	Methylene Blue	51.1/60	500	[49]
Mn_3O_4- MnO_2	Methylene Blue	93.5/60	500	[49]
HNTs/δ-MnO_2	Methylene Blue	97/60	40	[50]
Meso-MnO_2 - MCM-41	Methylene Blue	99/60	1000	[51]
Pelagite	Methylene Blue	98/100	3000	[52]

3D MnO_2 nanofibrous mesh	Methylene Blue	97/90	200	[53]
$CaFe_2O_3$	Methylene Blue	90/700	500	[54]
Fe_3O_4-coated biochar	Methylene Blue	93/180	400	[55]
Fe_3O_4/ZnO	Methylene Blue	94/60	200	[56]
Fe_3O_4/CRC	Methylene Blue	42/90	100	[56]
ZnO	Methylene Blue	58/120	1000	[57]
ZnO	Eosin Y	39/120	1000	[57]
A-ZIF-8	Rhodamine B	70/180	500	[58]

References:

1. U. N. Pan, V. Sharma, T. Kshetri, T. I. Singh, D. R. Paudel, N. H. Kim and J. H. Lee, *Small*, 2020, **16**, 2001691.
2. S. Ardizzone, G. Fregonara and S. Trasatti, *Electrochimica Acta*, 1990, **35**, 263-267.
3. J. Wang, J. Polleux, J. Lim and B. Dunn, *The Journal of Physical Chemistry C*, 2007, **111**, 14925-14931.
4. U. Latif, M. A. Raza, Z. U. Rehman, J. Iqbal, N. Lee, S. M. Z. Mehdi, M. F. Maqsood and S. Hussain, *International Journal of Energy Research*, 2022, **46**, 9643-9666.
5. W. Pholauyphon, P. Charoen-amornkitt, T. Suzuki and S. Tsushima, *Journal of Energy Storage*, 2024, **98**, 112833.

6. I. Rabani, J. Yoo, H.-S. Kim, S. Hussain, K. Karuppasamy and Y.-S. Seo, *Nanoscale*, 2021, **13**, 355-370.

7. Z. Zhu, Z. Wang, Z. Yan, R. Zhou, Z. Wang and C. Chen, *Ceramics International*, 2018, **44**, 20163-20169.

8. C. J. Raj, M. Rajesh, R. Manikandan, J. Y. Sim, K. H. Yu, S. Y. Park, J. H. Song and B. C. Kim, *Electrochimica Acta*, 2017, **247**, 949-957.

9. S. Li, J. Wen, X. Mo, H. Long, H. Wang, J. Wang and G. Fang, *Journal of Power Sources*, 2014, **256**, 206-211.

10. C.-K. Sim, S. R. Majid and N. Z. Mahmood, *Journal of Alloys and Compounds*, 2019, **803**, 424-433.

11. X. He, J. E. Yoo, M. H. Lee and J. Bae, *Nanotechnology*, 2017, **28**, 245402.

12. G. Sun, L. Ma, J. Ran, X. Shen and H. Tong, *Journal of Materials Chemistry A*, 2016, **4**, 9542-9554.

13. N. I. Chandrasekaran, H. Muthukumar, A. D. Sekar, A. Pugazhendhi and M. J. J. o. M. L. Manickam, 2018, **266**, 649-657.

14. J. S. Lee, C. Lee, J. Jun, D. H. Shin and J. Jang, *Journal of Materials Chemistry A*, 2014, **2**, 11922-11929.

15. X. Xiao, B. Han, G. Chen, L. Wang and Y. Wang, *Scientific reports*, 2017, **7**, 1-13.

16. M. Qorbani, T.-c. Chou, Y.-H. Lee, S. Samireddi, N. Naseri, A. Ganguly, A. Esfandiar, C.-H. Wang, L.-C. Chen and K.-H. Chen, *Journal of Materials Chemistry A*, 2017, **5**, 12569-12577.

17. J. Li, C. Zhao, Y. Yang, C. Li, T. Hollenkamp, N. Burke, Z.-Y. Hu, G. Van Tendeloo and W. Chen, *Journal of Alloys and Compounds*, 2019, **810**, 151841.

18. Y. Wang, W. Zhang, X. Guo, K. Jin, Z. Chen, Y. Liu, L. Yin, L. Li, K. Yin and L. Sun, *ACS applied materials & interfaces*, 2019, **11**, 7946-7953.

19. H. Fu, Y. Liu, L. Chen, Y. Shi, W. Kong, J. Hou, F. Yu, T. Wei, H. Wang and X. Guo, *Electrochimica Acta*, 2019, **296**, 719-729.

20. P. Howli, S. Das, S. Sarkar, M. Samanta, K. Panigrahi, N. S. Das and K. K. Chattopadhyay, *ACS omega*, 2017, **2**, 4216-4226.

21. X. Lu, X. Huang, S. Xie, T. Zhai, C. Wang, P. Zhang, M. Yu, W. Li, C. Liang and Y. Tong, *Journal of Materials Chemistry*, 2012, **22**, 13357-13364.

22. M. Gao, W.-K. Wang, Q. Rong, J. Jiang, Y.-J. Zhang and H.-Q. Yu, *ACS applied materials & interfaces*, 2018, **10**, 23163-23173.

23. C. Guan, X. Liu, W. Ren, X. Li, C. Cheng and J. Wang, *Advanced Energy Materials*, 2017, **7**, 1602391.

24. J. Zhang, J. Lin, J. Wu, R. Xu, M. Lai, C. Gong, X. Chen and P. Zhou, *Electrochimica Acta*, 2016, **207**, 87-96.

25. S. Nagamuthu and K.-S. Ryu, *Scientific reports*, 2019, **9**, 1-11.

26. C.-h. Tang, X. Yin and H. Gong, *ACS applied materials & interfaces*, 2013, **5**, 10574-10582.

27. R. Zeng, Z. Li, L. Li, Y. Li, J. Huang, Y. Xiao, K. Yuan and Y. Chen, *ACS Sustainable Chemistry & Engineering*, 2019, **7**, 11540-11549.

28. T. N. Khawula, K. Raju, P. J. Franklyn, I. Sigalas and K. I. Ozoemena, *Journal of Materials Chemistry A*, 2016, **4**, 6411-6425.

29. Y. Jia, H. Wan, L. Chen, H. Zhou and J. Chen, *Journal of Power Sources*, 2017, **354**, 1-9.

30. H. Ji, S. Hu, Z. Jiang, S. Shi, W. Hou and G. Yang, *Electrochimica Acta*, 2019, **299**, 143-151.

31. X. Xu, W. Zhong, X. Zhang, J. Dou, Z. Xiong, Y. Sun, T. Wang and Y. Du, *Journal of colloid and interface science*, 2019, **543**, 147-155.

32. T. Xue, Y. Yang, X.-H. Yan, Z.-L. Zou, F. Han and Z. Yang, *Materials Research Express*, 2019, **6**, 095029.

33. F. Guan, S. Chen, N. Sheng, Y. Chen, J. Yao, Q. Pei and H. Wang, *Chemical Engineering Journal*, 2019, **360**, 829-837.

34. K. Sharma, K. Pareek, R. Rohan and P. Kumar, *International Journal of Energy Research*, 2019, **43**, 604-611.

35. Z. Zou, W. Xiao, Y. Zhang, H. Yu and W. Zhou, *Applied Surface Science*, 2020, **500**, 144244.

36. J. Xing, P. Tao, Z. Wu, C. Xing, X. Liao and S. Nie, *Carbohydrate polymers*, 2019, **207**, 447-459.

37. K. Singh, S. Kumar, K. Agarwal, K. Soni, V. R. Gedela and K. Ghosh, *Scientific reports*, 2017, **7**, 1-12.

38. J. Wu, J. Peng, Z. Yu, Y. Zhou, Y. Guo, Z. Li, Y. Lin, K. Ruan, C. Wu and Y. Xie, *Journal of the American Chemical Society*, 2018, **140**, 493-498.

39. X. Hu, W. Shao, X. Hang, X. Zhang, W. Zhu and Y. Xie, *Angewandte Chemie International Edition*, 2016, **55**, 5733-5738.

40. S. S. Karade and B. R. Sankapal, *ACS Sustainable Chemistry & Engineering*, 2018, **6**, 15072-15082.

41. S. S. Karade and B. R. Sankapal, *Journal of Electroanalytical Chemistry*, 2017, **802**, 131-138.

42. M. S. Javed, S. Dai, M. Wang, D. Guo, L. Chen, X. Wang, C. Hu and Y. Xi, *Journal of Power Sources*, 2015, **285**, 63-69.

43. S. Zhao, W. Xu, Z. Yang, X. Zhang and Q. Zhang, *Electrochimica Acta*, 2020, **331**, 135265.

44. R. K. Mishra, A. K. Kushwaha, S. Kim, S. G. Seo and S. H. Jin, *Current Applied Physics*, 2019, **19**, 1-7.

45. I. Rabani, C. Bathula, R. Zafar, M. S. Tahir, Y.-J. Park, H.-S. Kim, M. Naushad and Y.-S. Seo, *Journal of Colloid and Interface Science*, 2022, **608**, 2347-2357.

46. P. Jing, J. Li, L. Pan, J. Wang, X. Sun and Q. Liu, *Journal of hazardous materials*, 2015, **284**, 163-170.

47. M.-X. Zhu, Z. Wang, S.-H. Xu and T. Li, *Journal of hazardous materials*, 2010, **181**, 57-64.

48. L. Zhang, J. Lian, L. Wu, Z. Duan, J. Jiang and L. Zhao, *Langmuir*, 2014, **30**, 7006-7013.

49. J. Zhao, J. Nan, Z. Zhao, N. Li, J. Liu and F. Cui, *Applied Catalysis B: Environmental*, 2017, **202**, 509-517.

50. S. Das, A. Samanta and S. Jana, *ACS Sustainable Chemistry & Engineering*, 2017, **5**, 9086-9094.

51. B. Nanda, A. C. Pradhan and K. Parida, *Microporous and Mesoporous Materials*, 2016, **226**, 229-242.

52. M.-X. Zhu, Z. Wang and L.-Y. Zhou, *Journal of hazardous materials*, 2008, **150**, 37-45.

53. M. Rahmat, A. Rehman, S. Rahmat, H. N. Bhatti, M. Iqbal, W. S. Khan, S. Z. Bajwa, R. Rahmat and A. Nazir, *Journal of Materials Research and Technology*, 2019, **8**, 5149-5159.

54. W. Shi, Q. Li, S. An, T. Zhang and L. Zhang, *Journal of Chemical Technology & Biotechnology*, 2016, **91**, 367-374.

55. P. Sun, C. Hui, R. A. Khan, J. Du, Q. Zhang and Y.-H. Zhao, *Scientific reports*, 2015, **5**, 1-12.

56. V. D. Doan, T. T. N. Le, M. U. Dao, T.-T. T. Vo, H. H. Do, D. Q. Viet and V. A. Tran, *Materials Letters*, 2021, **283**, 128749.

57. S. Chakrabarti and B. K. Dutta, *Journal of hazardous materials*, 2004, **112**, 269-278.

58. S. Wang, L. Luo, Z. Li, C. Jin, N. Wang, D. Wang, A. Wu, H. Yan, L. Wang and C. Tian, *Journal of Hazardous Materials*, 2022, **430**, 128501.